Middle-East Journal of Scientific Research 23 (12): 2968-2982, 2015
ISSN 1990-9233

DOI: 10.5829/idosi.mejsr.2015.23.12.10234

Histological, Immunohistochemical and Ultrastructural Study on the Effect of Gold Nanoparticles on the Left Ventricular Cardiac Myocytes of Adult Male Albino Rat

[1]Ebtsam F. Okasha and [2]Ayah Mohamed Hassan Ragab

[1]Department of Histology, Faculty of Medicine, Tanta University, Egypt
[2]Reproductive Health and Family Planning Department, National Research Centre, Giza, Egypt

Abstract: Gold nanoparticles (GNPs) have potential applications in biomedicine, but one of the important concerns is about their safety. The data about the degree of toxicity of GNPs in-vivo is not enough to judge. Aim of the work was to study the effect of GNPs on the histological structure of the cardiac muscle. *Materials and Methods*: 30 healthy male albino rats were randomly divided into 3groups including: control group (group I) and two GNPs-treated groups (group II received low dose (40ug/kg) and group III received high dose (400ug/kg) daily for 14 days). After the end of the experiment, all the rats were sacrificed; cardiac muscle was separated and processed to be examined by light and electron microscopy. *Results*: revealed that in GNPs induced various histological alterations including congested heart muscle with dilated blood vessels, extravasations of red blood cells, muscle hyalinosis, disturbed muscle fascicles and highly significant increased Caspase- 3 immunohistochemical reaction. These alterations were accompanied with ultra-structural changes as disruption and lysis of some myofibrils, degeneration of mitochondria, swelling in SER in addition to discontinuation and dilatation of intercalated discs. These changes were dose dependent as more destructive effects and damage have been observed at high concentration. In *Conclusions*: the histological alterations and results obtained from the present work might indicate that, GNPs exposure induced heart muscle damage which was dose dependent.

Key words: Gold Nanoparticles · Left Ventricle · Cardiac Myocytes · Rat · Histology, Immunohistochemistry · Ultrastructural

INTRODUCTION

Nanoparticles are important scientific tools that have been recruited in various biotechnological and pharmacological applications. They have two particular properties including their large surface area that dominates the contributions made by small bulk of the material and their quantum effects [1]. Gold nanoparticles (GNPs) are a tremendous scientific achievement of nanotechnology and are widely used in various fields of medicine and different industries such as agriculture, livestock, food packaging, beverages, toothpaste, automobiles, household appliances, cosmetic and disease treatment, these particles are also used in DNA detection [2, 3]. The use of NPs as drug carriers may reduce the toxicity of the incorporated drug [4]. Today, gold nanoparticles have been suggested to be potentially useful as a novel radio-sensitizer in radiotherapy, because the strong photoelectric absorption and secondary electron caused by gamma or X-ray irradiation can accelerate DNA strand breaks [5, 6].

Gold in its bulk form has been considered an inert, noble metal with some therapeutic and medicinal value. GNPs are thought to be relatively non-cyto-toxic [7], while the metallic nature of metal-derived NPs and the presence of transition metals encourages oxygen species (ROS), leading to the production of reactive oxidative stress [8]. There are differing reports of the extent of the toxic nature of these particles owing to the different modifications of the GNPs, surface functional attachments, shape and diameter size of the NPs [9, 10]. Considering the development of nanotechnology and extensive use of nano-materials in different fields of industry, it is necessary to investigate their destructive effects on biological systems.

Corresponding Author: Ebtsam F. Okasha, Department of Histology, Faculty of Medicine, Tanta University, Egypt.
E-mail: ebtsamokasha@gmail.com.

Extreme changes in the histopathology of lung and liver tissues caused by spherical GNPs were proved by some studies [11]. Cardiac tissue histological alterations due to the administration of GNPs have not been previously documented. In the present study, an attempt was made to characterize cardiac tissue histological alterations after administration of GNPs with various doses.

Due to the important uses of GNPs in biological and medical systems, the risk of toxic effects and the limited number of studies on its toxic effects, it seems that studies on the side effects of GNPs in vivo condition have particular importance. This study aimed to examine the toxic effects of GNPS on heart tissue.

MATERIALS AND METHODS

Chemicals

Gold Nanoparticles (GNPs)

Preparation of GNPs: The preparation of the GNPs followed the stander citrate –reduction route using Turkevich protocol [12, 13]. In brief 0.1699 g of gold salt (HAuCL4) was added to 100 ml of water producing a faint yellowish solution, this solution was boiled for 45 min forming 0.5 $x10^{-3}$ Mol dm -3 of $HAuCL_4.H_2O$ .1ml of this solution was transferred to 18 ml of the double distilled water in a conical flask for heating and stirred vigorously, when its temperature reached to the boiling point one milliliter of 0.5% sodium citrate as a reducing agent was quickly added. The color of the solution gradually changed from the initial faint yellow to clear, grey, purple and tantalizing wine red color of GNPs solution. Heating continued for another 15 min after that the solution was removed from the heater and stirred for further 15 min and was stored at 4°C in order to prevent aggregation. This method produces mono-disperse spherical gold nanoparticles in the range of 10–20 nm in diameter.

Animals: Thirty adult male albino rats, weighing 150-200 gm were used in this study. They were housed in standard environmental condition and allowed free access to water and food (in animal house -National Research Center Egypt).

Experimental Protocol: Rats Were Divided into 3 Groups, Each Group Included 10 Rats:

Group (I) Served as a Control Group: The animals of this group received no treatment.

Group (II) [GNPs Low Dose]: The animals of this group received a low dose (40ug/kg) of GNPs orally once per day for 14 days.

Group (III) [GNPs High Dose]: The animals of this group received a high dose (400ug/kg)[14] of GNPs orally once per day for 14 days.

Previous study reported that the oral administration route of GNPS produced the highest toxicity compared with intra-peritoneal and tail vein injection [15]. The animals were sacrificed by cervical dislocation on the next day at the end of the dosing period and then heart of each animal was dissected. Specimens from the cardiac wall at the left ventricular were excised. The experiment was approved by the Local Ethics Committee of Faculty of Medicine, Tanta University (Egypt).

Histological Study: Left ventricular specimens were fixed in 10% neutral buffered formalin and processed to obtain paraffin sections of 5-µm thickness to be stained with hematoxylin and eosin (H&E), Mallory Trichrome (MT) [16] and Congo red stains. Histological sections were examined by light microscope to assess the degree of cardiac affection [17, 18].

Immunohistochemical Study: for detection of caspase3 reaction in cardiac myocyte using an anti-caspase3 antibody. Sections were incubated with the primary rabbit anti-caspase3 overnight at 4°C. Primary binding was detected using a horseradish peroxidase-conjugated goat anti-rabbit antibody (Vector Laboratories, Burlingame, CA, USA) and visualized by development with 3, 3-diaminobenzidine (DAB, Sigma). All sections were counterstained with heamatoxylin. It appears as zymogen granules in the cytoplasm of cardiac myocyte [19].

Electron Microscopic Study: Small pieces ($1mm^3$) from the left ventricle were excised to be used for electron microscopy. Specimens were immediately fixed in 2.5% glutaraldehyde for 24 hours. Specimens were washed in 0.1 M phosphate buffer at 4°C, then post fixed in 1% osmium tetroxide at room temperature. Specimens were dehydrated in ascending grades of ethyl alcohol and then embedded in Epon resin. Semi-thin sections (1µm) were stained with toluidine blue (TB) and examined with light microscope. Ultrathin sections were cut, mounted on copper grids and stained with uranyl acetate and lead

citrate [20]. Specimens were examined and photographed with JEM transmission electron microscope in EM unite faculty of medicine, Tanta university.

Quantitative and Statistical Study: Optical density of caspase 3 immunoreactivity.

The image analysis system (Leica Q 500 MC Program; Leica, Switzerland) in the Tanta Faculty of Medicine Central Research Lab, Tanta, was used to measure the mean total optical density of desmin positive immunoexpression.

Statistical Analysis: The values were represented as mean ±SD. The data were analyzed, calculated and compared between groups using SPSS software (Chicago, USA). Differences were regarded significant if P value was less than 0.05 and highly significant if P value was less than 0.01.

RESULTS

Light Microscopic Findings

H&E Stain

Group I: (Control Group): H&E stained sections of control myocardium of the left ventricle showed normal histological structure of cardiac myocytes with their acidophilic sarcoplasm and pale centrally placed nuclei (Fig. 1 A&B). In group II (GNPs low dose), examination of the myocardium revealed some degenerative changes with dilatation and congestion of some blood vessels (Fig. 2 A&B), extravasations of red blood cells and few mononuclear cellular infiltration (Fig. 3 A&B), these changes were associated with disturbed muscle fascicles, some foci of muscle hyalinosis (homogenous acidophilic areas of the sarcoplasm), sarcoplasmic vacuolization specially in the perinuclear region together with nuclear peripheralization and pyknosis (Fig. 4 A&B). While in group III (GNPs high dose), demonstrating myocardium with marked dilatation and congestion of blood vessels, intra- muscular hemorrhagic (Fig. 5 A&B), extravasations of red blood cells (Fig. 6 A&B) and mononuclear infiltrate associated with marked disturbed, disorganized, fragmented muscle fascicles with extensive muscle hyalinosis and pyknosis of the nuclei (Fig. 7 A&B).

Mallory's Trichrome (MT) Stain: With Mallory's trichrome stain cardiac myocytes of left ventricular sections from control group showed few collagen fibers in the endomysium between the cardiac muscle fibers (Fig. 8A, B).While sections from group II (GNPs low dose) revealed obvious increase in the collagen fibers, which appeared as dense, wavy, thick bundles in between the cardiac muscle fibers and around the dilated congested blood vessels (Fig. 8C, D). On the other hand sections obtained from group III (GNPs high dose) showed focal areas of increased collagen fibers replace some cardiac muscle fibers (Fig. 8E, F).

Congo Red Stain: The presence of amyloid deposits in sections of heart was investigated by Congo red staining. Examination of Congo red stained sections of control group revealed absence of amyloid deposits (Fig. 9A, B). While the amyloid deposition was identified by its characteristic red coloration in Congo red stained sections of myocardium of the left ventricle of group II (GNPs low dose) (Fig. 9C, D). As regard to Congo red stained sections of group III (GNPs high dose) revealed extensive amyloidosis. (Fig. 9E, F).

Immunostaining with Caspase 3 Antibody: The reaction appeared as fine brown granules in the sarcoplasm of cardiac myocytes of control groups ((Fig. 10A, B), however an apparent increase in the reaction was detected in sarcoplasm of the cardiac myocytes of both group II (GNPs low dose) (Fig. 10C, D) and group III (GNPs high dose) (Fig. 10E, F).

Electron Microscopic Finding: Examination of the ultrathin sections of the myocardium of the left ventricle of the control group showed the normal histological structure of the cardiac muscle fibers which appeared as striated fibers with regular arrangement of myofibrils. Each cardiac myocyte contained a central elongated euchromatic nucleus with a prominent nucleolus, sarcoplasm contained abundant mitochondria with closely packed cristae and uniformly distributed in rows between the myofibrils. Multiple step-like intercalated discs were detected attaching cardiac myocytes with each other (Fig. 11). Ultrathin sections of the myocardium of group II (received low dose of GNPs for 14 days) showed cardiac myocytes with disorganized, fragmented disrupted myofibrils with loss of their regular cross striations and some areas showed lysis, there were wide spaces which reflect the presence of edema in between the myofibrils, in addition to dilatation of SER and discontinuation of the intercalated discs (Fig. 12). The mitochondria were disarranged, variable in shape and size with partial distortion and disruption of their cristae (Fig. 13).

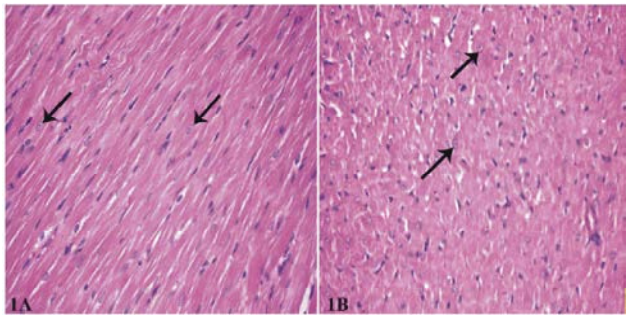

Fig. 1: Photomicrographs of the cardiac muscle from control rat sections showing cardiac myocytes with acidophilic sarcoplasm and pale centrally located nuclei in LS (1A) and TS (1B) sections of left ventricular muscle. H&E X 400

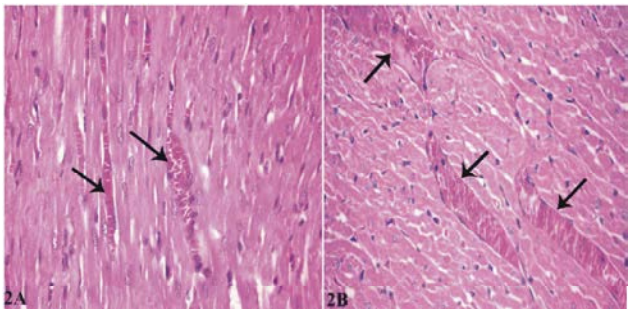

Fig. 2: Photomicrographs of the cardiac muscle from rats of group II (received low dose of GNPs for 14 days) showing cardiac muscle with prominent dilated congested blood vessels (→) in the LS (2A) and TS (2B) sections of left ventricular muscle. H&E X 400

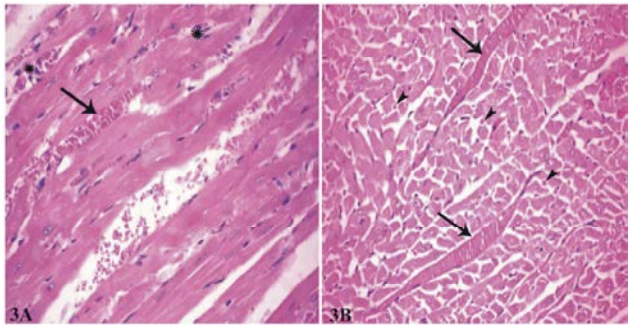

Fig. 3: Photomicrographs of the cardiac muscle from rats of group II showing congested dilated blood vessels (→) scattered and extravasations of red blood cells (▸) with small foci of mononuclear cellular infiltration (★) in LS (3A) and TS (3B) sections of left ventricular muscle. H&E X 400

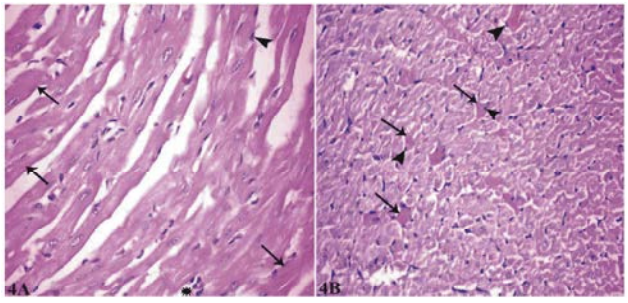

Fig. 4: Photomicrographs of the cardiac muscle from rats of group II showing foci of homogenous acidophilic sarcoplasm (→) together with nuclear peripheralization and pyknosis (▸) in LS (4A) and TS (4B) sections of left ventricular muscle. Notice: small foci of lymphocytic infiltration (★). H&E X 400.

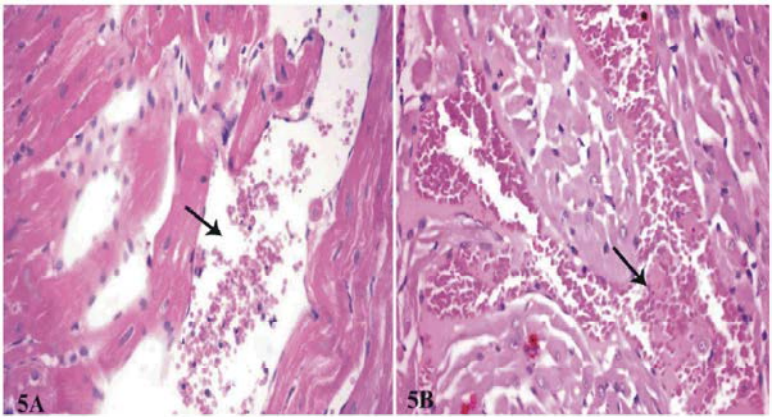

Fig. 5: Photomicrographs of the cardiac muscle from rats of group III (received high dose of GNPs for 14 days) showing prominent dilated congested blood vessels (→) in LS (5A) and TS (5B) sections of left ventricular muscle. H&E X 400

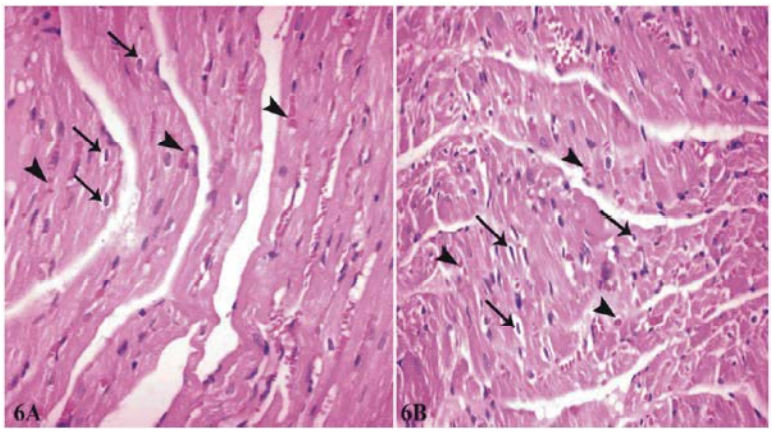

Fig. 6: Photomicrographs of the cardiac muscle from rats of group III showing extravasations of red blood cells (▸) sarcoplasmic vacuolization with pyknotic nuclei surrounded by empty spaces (→) in LS (6A) and TS (6B) sections of left ventricular muscle. H&E X 400

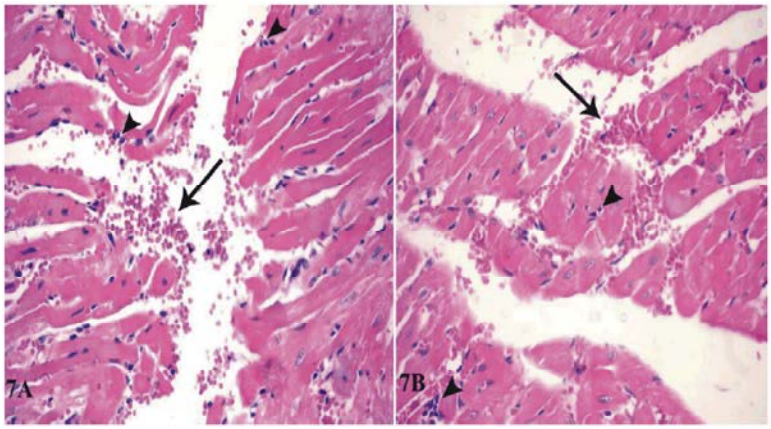

Fig. 7: Photomicrographs of the cardiac muscle from rats of group III disturbed disorganized, fragmented muscle fascicles with extensive muscle hyalinosis and pyknosis and peripheralization of the nuclei with inter-muscular hemorrhage (→) and some foci of mononuclear cellular infiltration (▸) in LS (A) and TS (B) sections of left ventricular muscle. H&E X 400

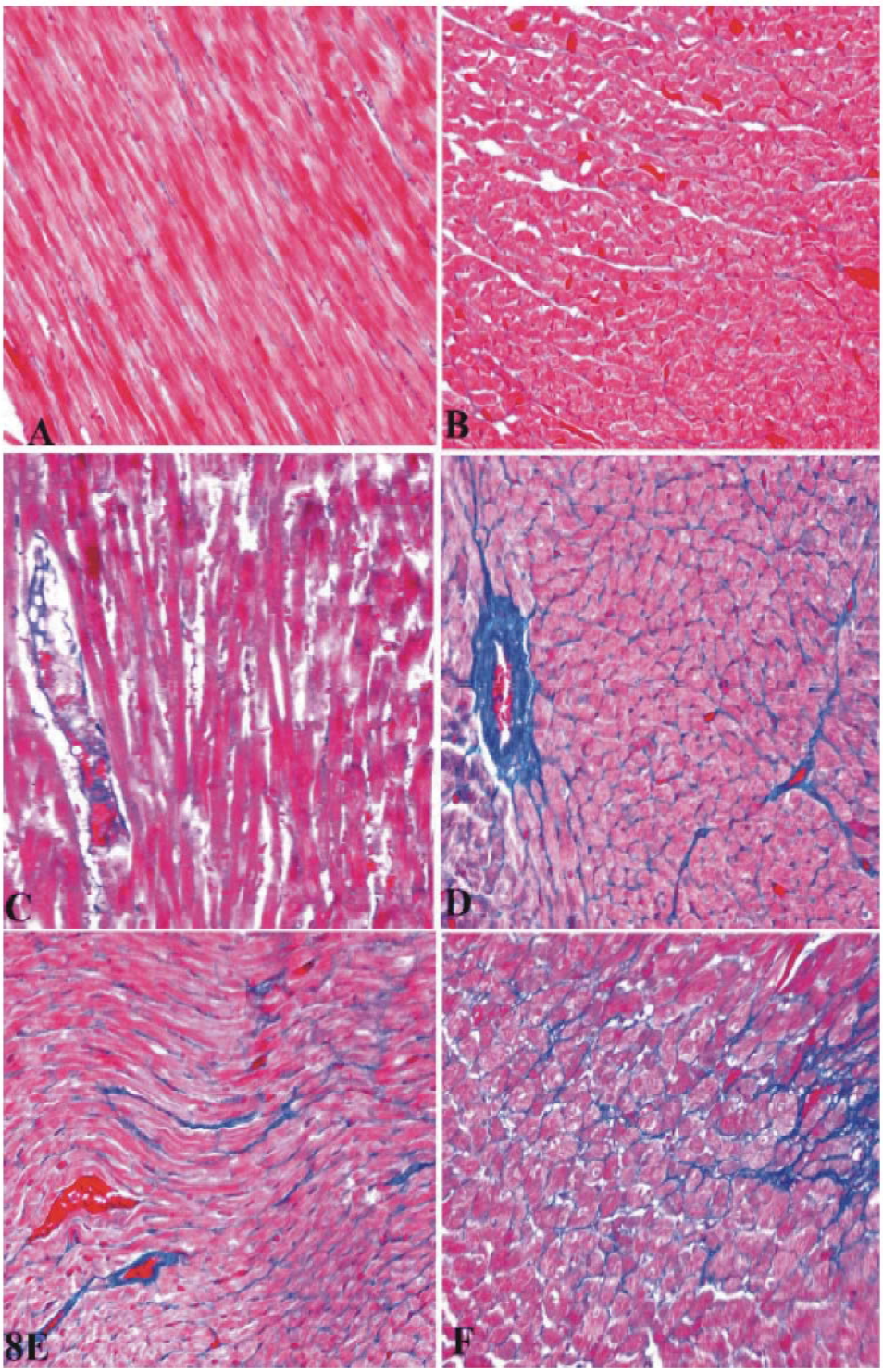

Fig. 8: Photomicrographs of left ventricle muscle sections showing few blue- stained collagen fibers between the cardiac muscle fibers of control group in LS(A)and TS (B)sections, increased amount of collagen fibers in between cardiac muscle fibers and around blood vessels of group II in LS(C)and TS(D) sections and large amount of collagen fibers which appear as dense, wavy, thick bundles in between the cardiac muscle fibers with focal areas of collagen fibers replace some degenerated cardiac myocytes in LS(E)and TS(F)sections sections. MT. stain x 400

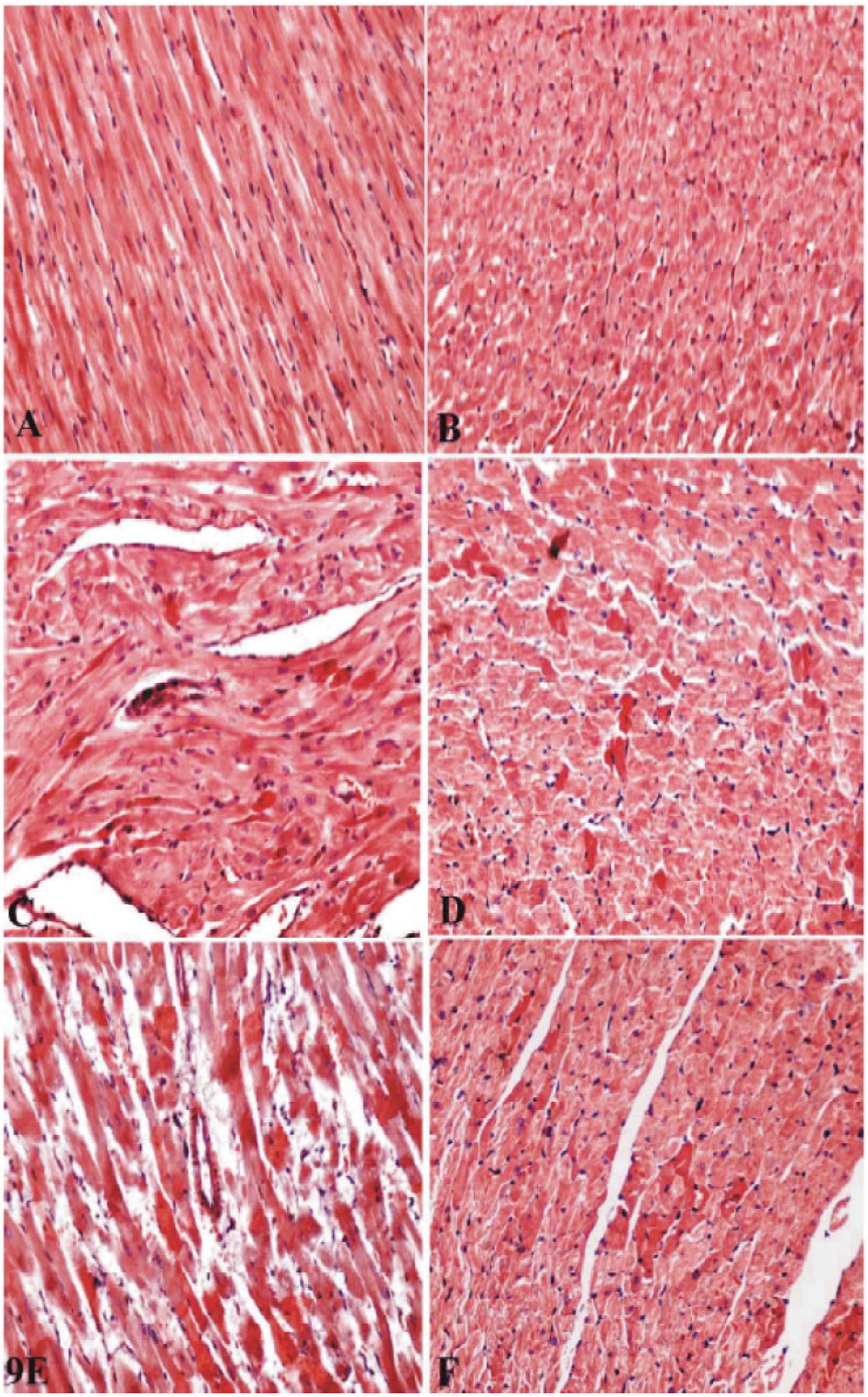

Fig. 9: Photomicrographs of left ventricle muscle sections showing no amyloid deposits in the cardiac muscle fibers of control group in LS(A)and TS (B)sections, red color amyloid deposits within some cardiac muscle fibers of group II in LS(C)and TS(D)sections and extensive amyloid deposits in many cardiac myocytes of group III in LS(E) and TS(F) sections. Congo red stain x400

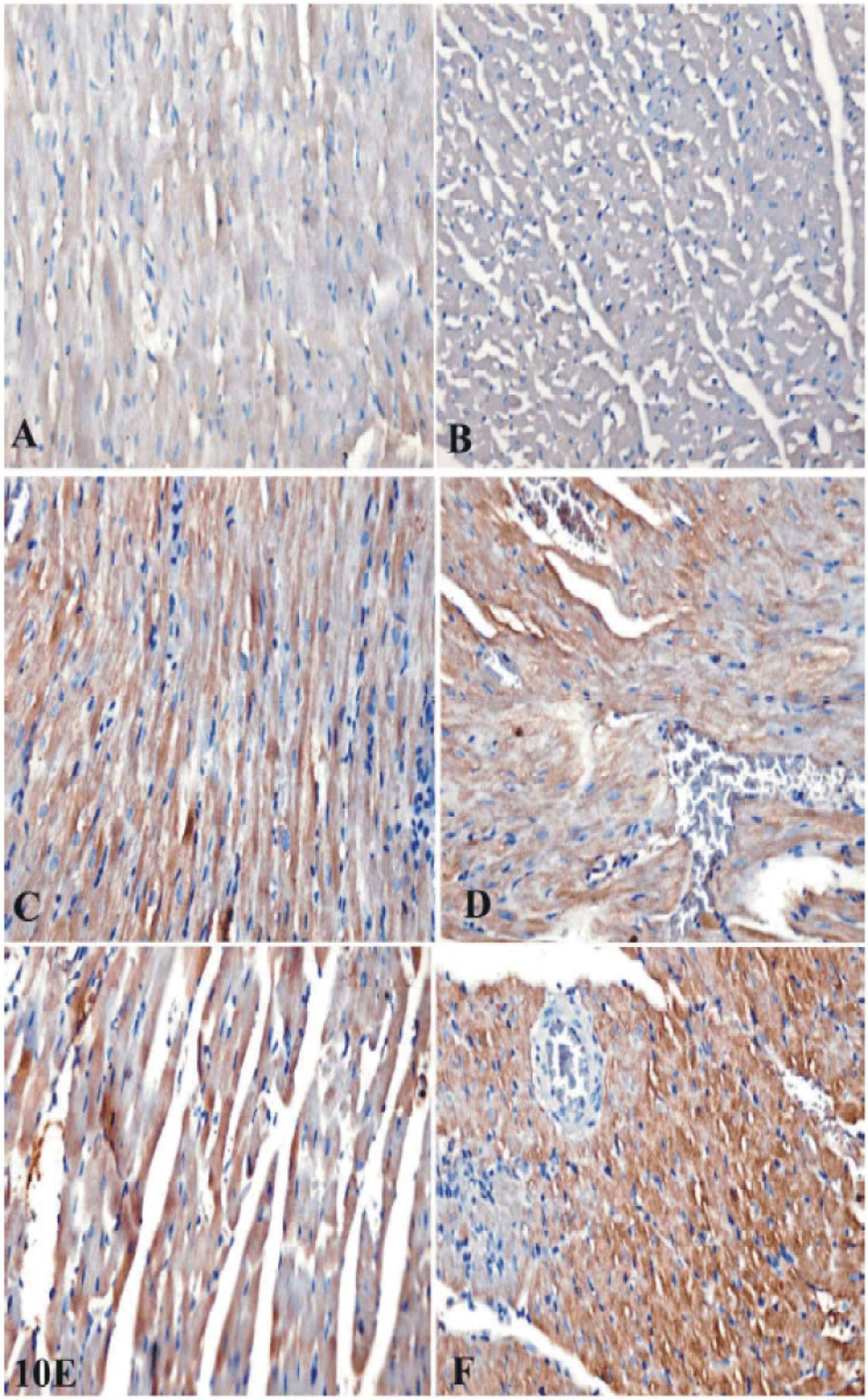

Fig. 10: Photomicrographs of left ventricle muscle sections showing faint brown staining granules in the sarcoplasm of cardiac myocytes of control group in LS(A)and TS(B)sections, more dark staining granules in sarcoplasm of group II in LS(C)and TS(D)sections and group III in LS (E)and TS (F)sections. Caspase 3-antibody & H×400

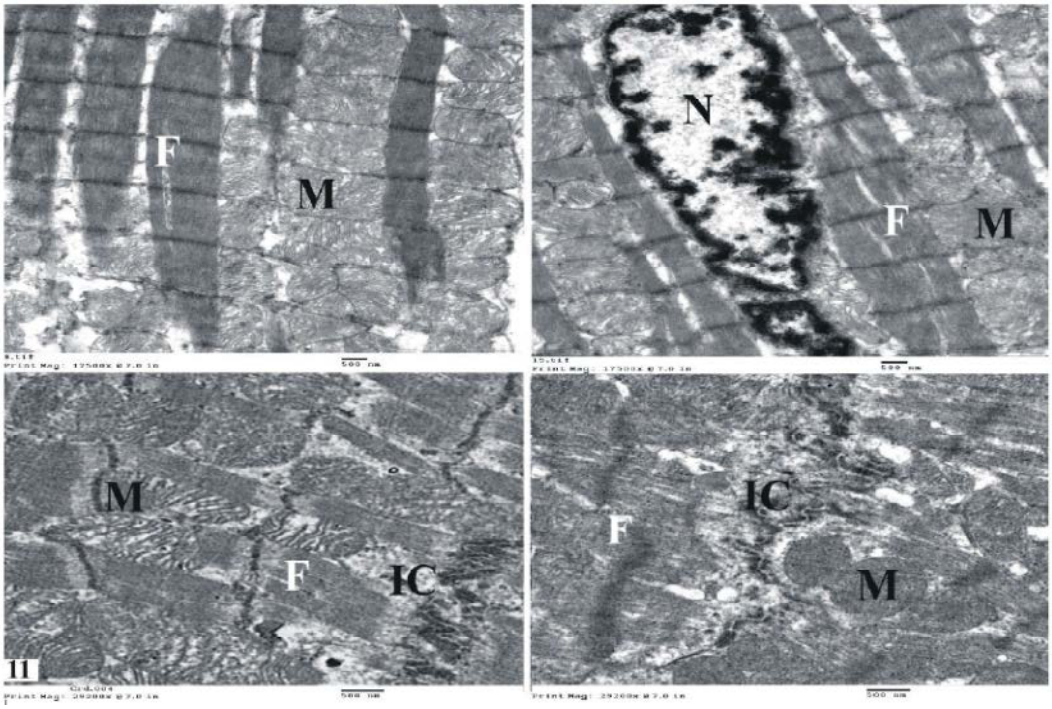

Fig. 11: Electron-micrographs of an ultrathin section of rats'left ventricular myocardium of control group showing, cardiac myocytes with regular arrangement of the myofibrils (F) oval euchromatic nuclei (N) abundant mitochondria (M) with regular arrangement, normal intercalated disc (IC) with multiple longitudinal and transverse portions

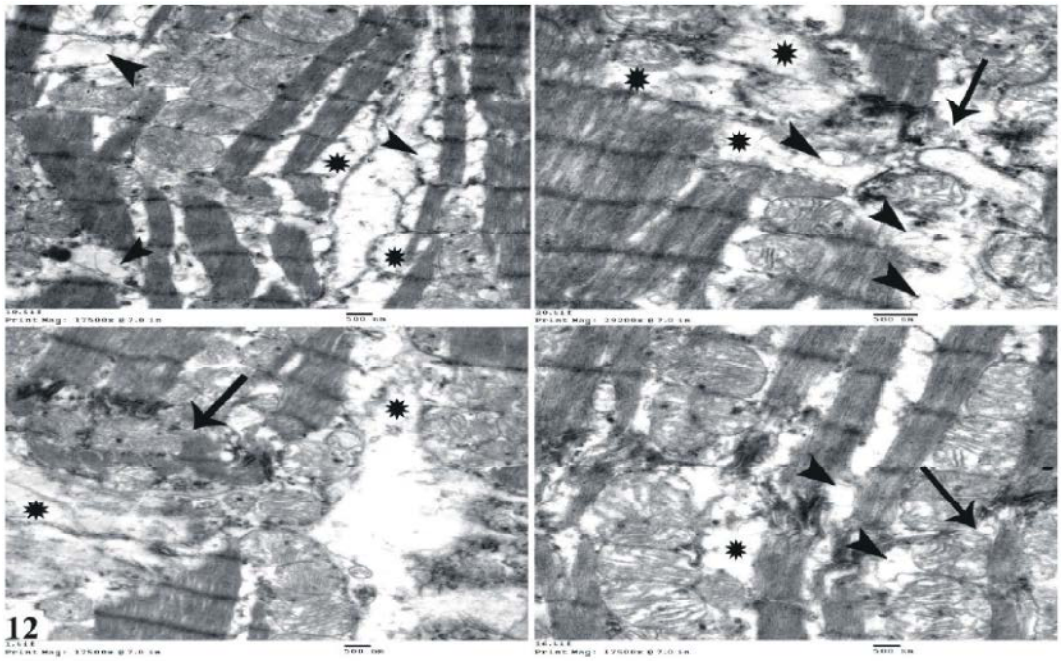

Fig. 12: Electron-micrographs of an ultrathin section of rats'left ventricular myocardium of group II(received low dose of GNPs for 14 days) showing disorganized, disrupted myofibrils with loss of their regular arrangement, some areas showing wide spaces (★) between the myofibrils, dilatation of SER (▸) and discontinuation (→) of the intercalated discs

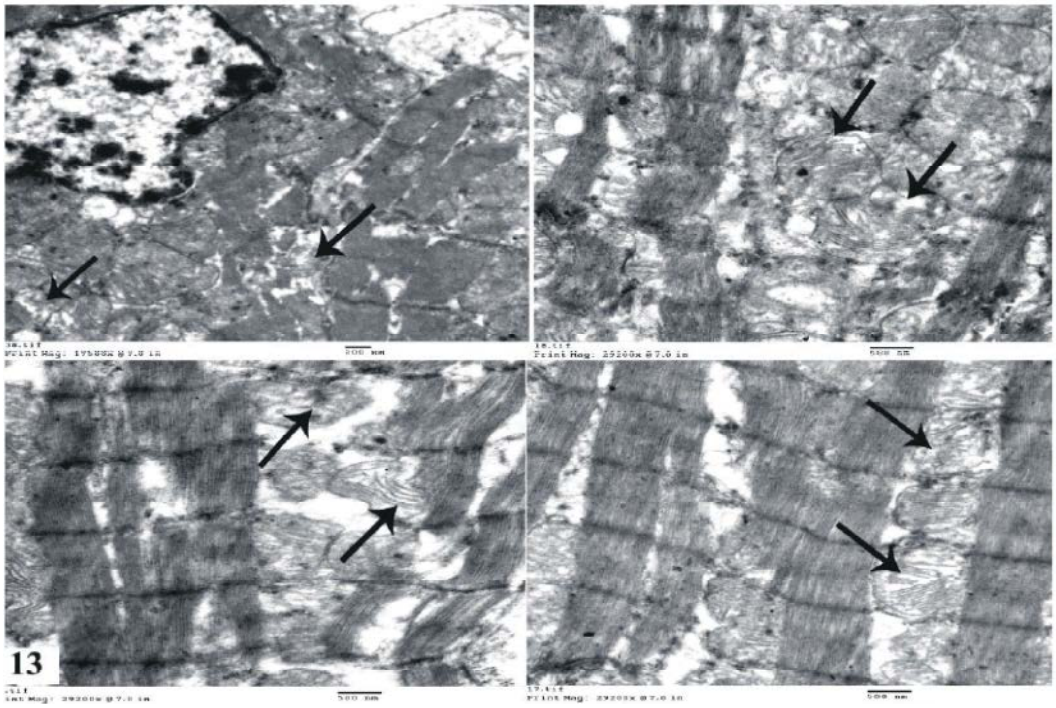

Fig. 13: Electron-micrographs of an ultrathin section of rats'left ventricular myocardium of group II showing disarranged, mitochondria with partial distortion and disruption of their cristae (→)

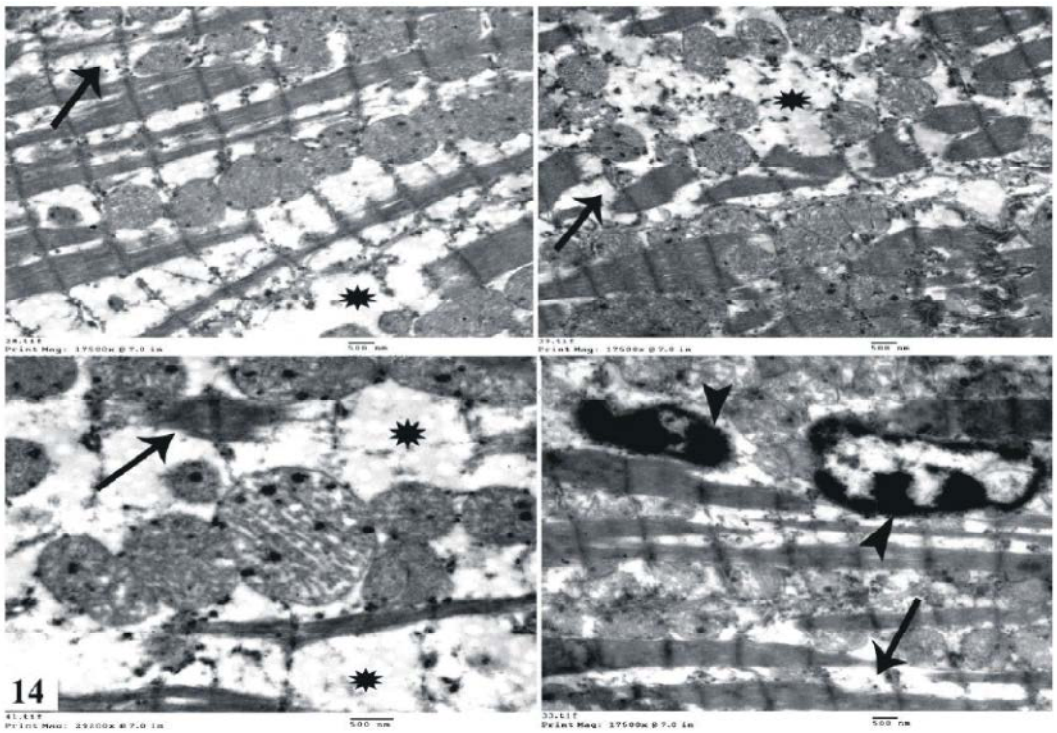

Fig. 14: Electron-micrographs of an ultrathin section of rats'left ventricular myocardium of group III(received high dose of GNPs for 14 days) showing extensive destruction and degeneration of the myofibrils with rarefaction (★) of the sarcoplasm, lysis of myofibrils (→) and some shrunken irregularly indented nuclei with electron dense chromatin (▸)

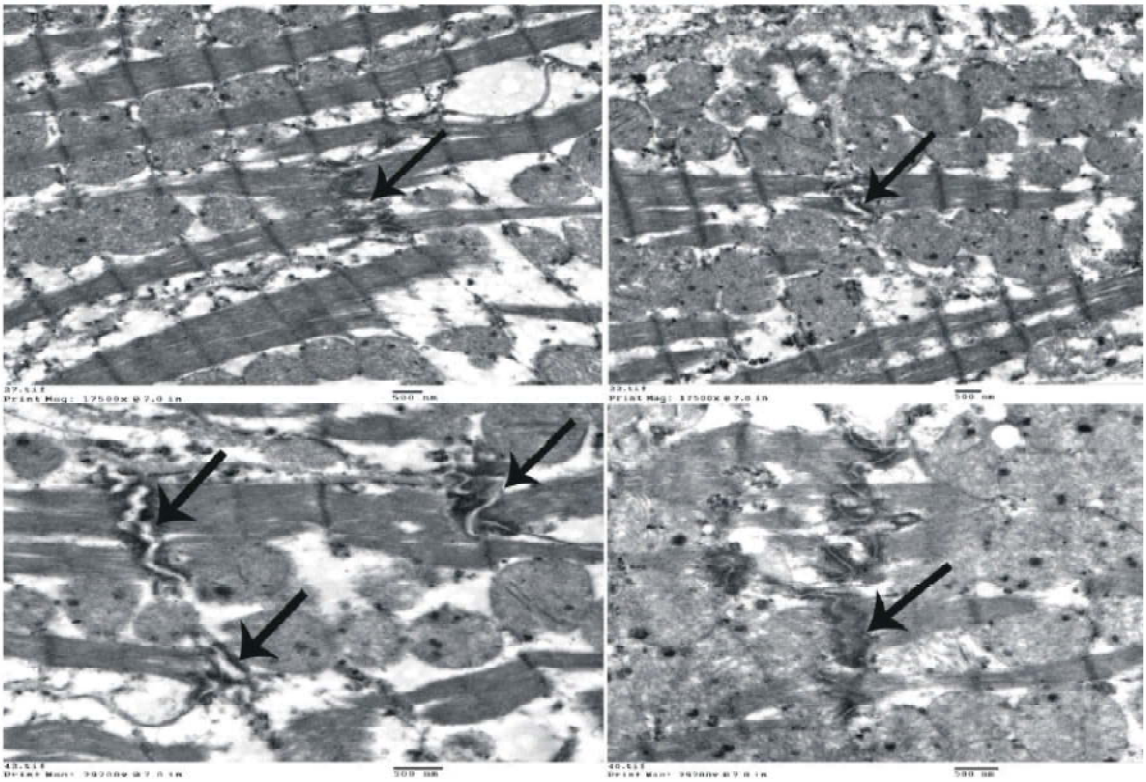

Fig. 15: Electron-micrographs of an ultrathin section of rats'left ventricular myocardium of group III showing dilatation and discontinuation of intercalated discs (→)

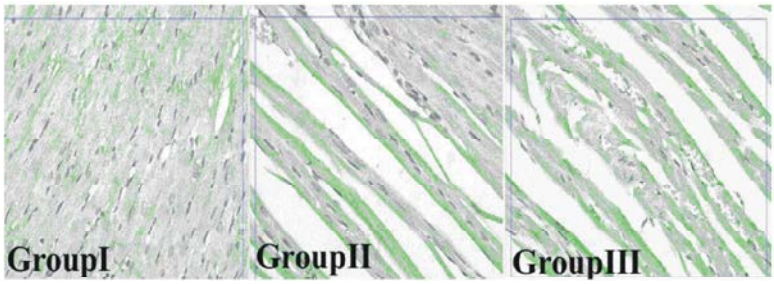

Fig. 16: Showing difference in the optical density of caspase3 immuno-expression of different groups

Table 1: Optic density for caspase3 immuno-staining

GROUPS	Mean± SD	T test	P value
Control	76.572±2.769	-	-
Low dose GNPS	84.188 ±2.410	5.487	0
High dose GNPS	87.644±1.499	9.30	0

Electron microscopic results of group III revealed marked degenerative changes in the cardiac myocytes. Extensive destruction and degeneration of the myofibrils and even complete lysis of myofibrils, rarefaction in the sarcoplasm and some shrunken irregularly indented nuclei with electron dense chromatin were observed (Fig. 14). Dilation and discontinuation of intercalated discs in some myocytes were also observed (Fig. 15). GNPS were observed as electron dense aggregates with different sizes in cardiac myocytes in between the myofibrils and related to the mitochondria and the sarcolemma mainly in group III than group II (Fig. 12-15).

Statistical Results for the Optical Density Caspase3 Immuno-Reactivity: Figure 16, Table 1 and histogram 1, showed that, there was significant difference in the mean values of optical density of caspase3 immuno-expression in all studied groups. There was a high significant difference (P<0.000) between the three studied groups; both low dose GNPS treated group and high dose GNPS had high significant increase as compared with control group.

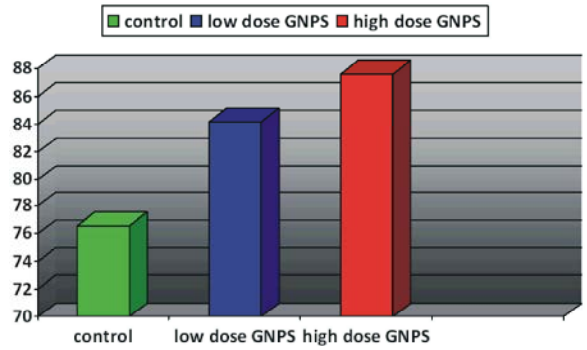

Histogram 1: Showing the mean value of caspase 3 immunostaining of different groups

DISCUSSION

With this increase in consumer products containing GNPS, the potential for worker exposure to GNPS will also increase. On the other hand only a few studies have been performed on the in vivo toxicology of GNPS. However, the potential toxicity of GNPS is still not completely understood, several mechanisms for cardiotoxicity have been reported, one of the most accepted mechanisms is through formation of the free radicals, that cause membrane and macromolecules damage which directly lead to myocardial damage [21].

The myocardial damage was detected in this research in the form of congestion of blood vessels, hemorrhage, excess extravasations of red blood cells in between cardiac myocytes, disruption and degenerative changes of cardiac muscle fibers, mitochondrial degeneration, dilatation of SER, vacuolation in the cytoplasm, destruction and even lysis of the myofibrils in addition to dilatation and discontinuation of intercalated discs. More damage was detected with high dose GNPs exposure.

The present findings were in the same line with those reported by other authors [22-23] who suggested that the main mechanism of toxicity of GNPs is through oxidative stress that causes damage to the lipids, carbohydrates, protein and DNA. The findings of the present research were also supported by many studies that reported that, the appearance of congested heart muscle with prominent dilated blood vessels and some foci of mononuclear cells infiltrate may suggest that GNPs interact with proteins and enzymes of the tissue interfering with the antioxidant defense mechanism and leading to reactive oxygen species (ROS) generation which in turn may induce stress, ROS production could result from the proportionately high surface area of GNPs [24-25].

As regards to the interstitial hemorrhage that observed in this study was previously explained by some investigators [26] to be due to tissue hypoxia which induces increase in capillary permeability. Congestion and dilatation of the blood vessels may be due to the direct effect of GNPS on the endothelial cells of the blood vessels leading to the release of endothelial relaxation factor nitric oxide (NO) with subsequent vasodilatation.

In the present research scattered cytoplasmic vacuolization that appeared in the current study was explained as a result of disturbances of membranes function that caused by GNPS leads to massive influx of water and Na+. This explanation was supported by others investigators who mentioned that formation of vacuoles might be explained by expansion of cytoplasmic membranous components caused by intracellular water and electrolytes redistribution [27]. Some authors added that, cellular swelling might be accompanied by leakage of lysosomal hydrolytic enzymes that lead to cytoplasmic degeneration and macromolecular crowding [28].

In the current study degeneration of cardiomyocytes was detected in H&E stained sections in the form of homogenous highly acidophilic (hyalinization) sarcoplasm, in Congo red sections as homogenous red stained areas and loss of striations in ultrathin sections. It has been well known, that Congo red staining is one of the powerful methods for the identification of amyloid degeneration [17]. Degeneration of cardiac myocytes may occur as a result of increased protein degradation and decreased myofibrillar protein synthesis. Accumulation of reactive free radicals might facilitate the release of lysosomal enzymes into the cytosol with subsequent oxidation of the protein backbone of these myofibrils causing their fragmentation [29].

Nuclear changes were observed in this research as pyknosis, pripheralization and degeneration. It has been long believed that apoptosis does not occur in terminally differentiated cells such as adult cardiac myocytes; however, all mechanisms responsible for induction of apoptosis were occurring in myocytes and are particularly activated during heart stress or chemical toxicity. Furthermore mitochondrial oxidative damage can increase the tendency of mitochondria to release inter-membrane space proteins such as cytochrome C to the cytosol by mitochondrial outer membrane permeability and thereby activate the cell's apoptotic machinery. Consequently, mitochondria have a key role in caspase induced apoptosis [30] that can explain the increased caspase- 3 reactions in group III.

Mitochondria are important intracellular organelles, it was reported that when the mitochondria triggered, cell death through a cascade of events launched by apoptogenic proteins. The outer mitochondrial membrane is the last barrier between the mitochondrion and the cytoplasm, an increase in mitochondrial membrane permeability is one of the key events in apoptotic and necrotic death [31]. This was coincided with the results of the previous study that proved that, breaches of outer mitochondrial membrane integrity result in the release of cytochrome C oxidase, triggering apoptosis [32]. In this study mitochondrial changes were observed in the form of swelling, degeneration, abnormal shapes and disruption of the cristae, it was suggested that swelling of the mitochondria may lead to rupture of the outer membrane and release of cytochrome C, a strong activator of caspase which trigger the cell to undergo apoptosis [33].

The dilatation of the sarcoplasmic reticulum that appeared in the present work was also observed by other investigators [34] they attributed these changes to the low concentration of calcium in the cytoplasm close to the intercalated disc due to alteration of the mitochondria and sarcoplasmic reticulum membranes. However recent findings [35] postulated these changes due to the intracellular calcium overload that would over activate a series of calcium dependent protein kinase in the cytoplasm and cause serious impairment of cardiomyocyte membranes.

As regards to discontinuation, dilatation and abnormalities in the intercalated discs that observed in this research could be attributed to activation of lipid per-oxidation secondary to defective mitochondrial function that lead to breakdown of phospholipids including that of the biological membranes, which resulted in disturbed membrane structure, impaired function, inactivation of membrane receptors and enzymes with increased nonspecific permeability to ions [36].

In this study GNAPs were detected in cardiac tissue in between the myofibrils, mitochondria and related to sarcolemma. Such findings are in line with results of other investigators who mentioned that, the morphologic evidence provided by TEM indicates that NPs leave the capillary lumen, cross the endothelial layer, penetrate the sarcolemma and reach the sarcoplasm by establishing intimate contact with myofibrils and mitochondria [37]. For the visualization of electron-dense inorganic NP, TEM has been widely used to characterize the morphology and size of NP as well as their location in tissues, however that artifacts due to staining with lead citrate and uranyl acetate can easily be misinterpreted as NP [38]. Other authors reported that, the 10 nm particles were detected in various organ systems including blood, liver, spleen, kidney, testis, thymus, heart, lung and brain, whereas the larger particles were only detected in the blood, liver and spleen. These results demonstrate that tissue distribution of gold nanoparticles is size-dependent, with the smallest (10 nm) nanoparticles showing the most widespread organ distribution [39].

CONCLUSION

The histological alterations and results obtained from the present work might indicate heart muscle damage by GNPs exposure. On the other hand, worldwide use of different GNPs requires more accurate studies on the effects of these nanoparticles with different concentrations and shapes on different organs of the body.

ACKNOWLEDGEMENTS

The author would like to thank Dr. Awatiff EL-Shall, Professor of Histology, Faculty of Medicine, Tanta University, for her help and support.

Conflicts of Interest: There is no conflict of interest to declare.

REFERENCES

1. Jae, H.S., H.J. Jun, D.P. Jung, Y.S. Moon, S.S. Kyung, R.R. Hyeon, Y. Jin, Uk, S.J. Ki, J. Jayoung, S.H. Beom, H.C. Yong, K.C. Hee, H.L. Ji, W.K. Dong, J.K. Bruce and Il Je Yu, 2011. Subchronic inhalation toxicity of gold nanoparticles. Particle and Fibre. Toxicology, 8:16 doi:10.1186/1743-8977- 8-16.
2. Manikandan, J., C.N. Ong, L.E. Yu and W.Y. Ong, 2010. Bio-distribution of gold nanoparticles and gene expression changes in the liver and spleen after intravenous administration in rats. Biomaterials., 31(8): 2034-2042.
3. Alkilany, A.M. and C.J. Murphy, 2010. Toxicity and cellular uptake of gold nanoparticles: What we have learned so far? J. Nanopart Res., 12(7): 2313-2333.
4. Kim, S.Y., Y.M. Lee, D.J. Baik and J.S. Kang, 2003. Toxic characteristics of methoxy poly (ethylene glycol)/ poly (ε-caprolactone) nanospheres; in vitro and *in vivo* studies in the normal mice. Biomaterials, 24: 55-63.

5. Hainfeld, J.F., D.N. Slatkin and H.M. Smilowitz, 2004. The use of gold nanoparticles to enhance radiotherapy in mice. Phys. Med. Biol., 49: N309-315.
6. Liu, C.J., C.H. Wang, C.C. Chien, T.Y. Yang, S.T. Chen, W.H. Leng, C.F. Lee, K.H.Lee, Y. Hwu, Y.C. Lee, C.L. Cheng, C.S. Yang, Y.J. Chen, J.H. Je, G. Margaritondo, 2008. Enhanced x-ray irradiation-induced cancer cell damage by gold nanoparticles treated by a new synthesis method of polyethylene glycol modification. Nanotechnol., 19: 295104-295109.
7. Mac Nee, W. and K. Donaldson, 2003. Mechanism of lung injury caused by PM10 and ultrafine particles with special reference to COPD. Eur. Respir J., 40: 47S-51S.
8. Jia, H.Y., Y. Liu, X.J. Zhang, L. Han, L.B. Du, Q. Tian and X. Yc, 2009. Potential oxidative stress of gold Nanoparticles by induced-NO releasing in serum. J. Am. Chem. Soc., 131(1): 40-1.
9. Takahashi, H., Y. Niidome, T. Niidome, K. Kaneko, H. Kawasaki and S. Yamada, 2006. Modification of gold nanorods using phosphatidylcholineto reduce cytotoxicity. Langmuir, 22(1): 2-5.
10. Pan, Y., S. Neuss, A. Leifert, M. Fischler, F. Wen, U. Simon, G. Schmid, W. Brandau and W. Jahnen-Dechent, 2007. Size-dependent cytotoxicity of goldnanoparticles. Small, 3(11): 1941-1949.
11. Monir Doudi and Mahbubeh Setorki, 2014. The acute liver injury in rat caused by gold nanoparticles. Nanomed J. Summer., 1(4): 248-257.
12. Turkevich, J., P.C. Stevenson and J. Hillier, 1951. A study of the nucleation and growth processes in the synthesis of colloidal gold. Discuss Faraday Soc., 11: 55-75.
13. Kara, Z., E.G. William, K. Sanjeev and D. Marie-Christine, 2012. Effect of high gold salt concentrations on the size and polydispersity of gold nanoparticles prepared by an extended Turkevich-Frens method. Gold Bull, 45: 203-211.
14. Lasagna, R.C., R.D. Gonzalez-, M.A. Barria, I. Olmedo, A. Clos, V.M. Sadagopa Ramanujam, A. Urayama, L. Vergara, M.J. Kogan and C. Soto, 2010. Bioaccumulation and toxicity of gold nanoparticles after repeated administration in mice. Biochem. Biophys Res. Commun., 393: 649-655.
15. Xiao-Dong Zhang, Hong-Ying Wu, Di Wu, Yue-Ying Wang, Jian-Hui Chang, Zhi-Bin Zhai, Ai-Min Meng, Pei-Xun Liu, Liang-An Zhang and Fei-Yue Fan, 2010. Toxicologic effects of gold nanoparticles in vivo by different administration routes . Int J Nanomedicine., 5: 771-781.
16. Bancroft, J.D. and M. Gamble, 2002. Theory and Practice of Histological Techniques, 5th edition, Churchill livingstone, Edinburgh, London, New York, Tokyo, pp: 139.
17. Nakanishi, T., M. Ito, T. Nirasawa, M. Tsuji and T. Takubo, 2013. Topologies of amyloidogenic proteins in Congo red-positive sliced sections of formalin-fixed paraffin embedded tissues by MALDI-MS imaging coupled with on-tissue tryptic digestion. Clin Biochem., 46: 1595-1600.
18. Jinping, L., L. Jie, Z. Peng, Z. Fang, S. Jingjing, Z. Peilan and S. Xuguo, 2014. Evidence of the presence of amyloid substance in the blood of familial amyloidotic polyneuropathy patients with ATTR Val 30 Met mutation Int J. Clin Exp. Pathol., 7(11): 7795-7800.
19. Burniston, J.G., A. Saini, L.B. Tan and D.F. Goldspink, 2005. Angiotensin II induces apoptosis in vivo in skeletal, as well as cardiac, muscle of the rat. Exp. Physiol., 90(5): 755-61.
20. Kuo J. Electron Microscopy, 2007. Methods and Protocols, 2nd ed. Humana Press Inc. Totowa, New Jersey, pp: 369.
21. Kim, S.Y., S.J. Kim, B.J. Kim, S.Y. Rah, S.M. Chung, M.J. Im and U.H. Kim, 2006. Doxorubicin-induced reactive oxygen species generation and intracellular Ca2+ increase are reciprocally modulated in rat cardiomyocytes. Exp. Mol. Med., 38(5): 535-545.
22. Mohamed Anwar K. Abdelhalim, 2011. Exposure to gold nanoparticles produces cardiac tissue damage that depends on the size and duration of exposure-Lipids in Health and Disease, 10: 205.
23. Abdelhalim, M.A.K., 2011. Gold nanoparticles administration induces disarray of heart muscle, hemorrhagic, chronic inflammatory cells infiltrated by small lymphocytes, cytoplasmic vacuolization and congested and dilated blood vessels. Lipids Health Dis., 10: 233.
24. Nel, A., T. Xia, L. Mädler and N. Li, 2006. Toxic potential of materials at the nano level. Science, 311: 622-627.
25. Pagan, I., D.L. Costa, J.K. McGee, J.H. Richards and J.A. Dye, 2003. Metals mimic airway epithelial injury induced by in vitro exposure to Utah Valley ambient particulate matter extracts. J. Toxicol. Environ. Health, 66A: 1087-1112.
26. Rashwan, S., M. Abd El Hafez, S. El Kalaawy and A. Abd El Mohsen, 1988. Effect of certain stress factors on the histology and histochemistry of rat kidney. Egypt. J. Histol., 11(1): 121-129.

27. Balli, E., U.O. Mete, A. Tuli, O. Tap and M. Kaya, 2004. Effect of melatonin on the cardiotoxicity of doxorubicin. Histol. Histopathol. Oct., 19(4): 1101-1108.
28. Del Monte, U., 2005. Swelling of hepatocytes injured by oxidative stress suggests pathological changes related to macromolecular crowding. Medical Hypotheses, 64(4): 818-825.
29. Tokunaga, T., S.R. Morshed, S. Otsuki, F. Takayama, T. Satoh, K. Hashimoto, T. Yasui, S. Ogawa, H. Kanegae, Y. Yokote, K. Akahane, M. Kashimata and Satoh K. Sakagami, 2003. Effect of antioxidants, oxidants, metals and saliva on cytotoxicity induction by sodium fluoride. Anticancer Res., 23(5A): 3719-3726.
30. Murphy, M.P., 2009. How mitochondria produce reactive oxygen species. Biochem. J., 417(1): 1-13.
31. Tsujimoto, Y., T. Nakagawa and S. Shimizu, 2006. Mitochondrial membrane permeability transition and cell death. Biochim. Biophys. Acta, 1757: 1297-1300.
32. Salnikov, V., Y.O. Lukya´nenko, C.A. Frederick, W.J. Lederer and V. Lukya´nenko, 2007. Probing the Outer Mitochondrial Membrane in Cardiac Mitochondria with Nanoparticles. Biophysical. Journal, 92: 1058-1071.
33. Green, D.R. and J.C. Reed, 1998. Mitochondria and apoptosis. Science (Washington D.C.); 281(5381): 1309-1311.
34. Soldani, P., A. Pellegrini, M. Gesi, P. Lenzi, R. Cristofani and A. Paparelli, 1997. SEM/TEM investigation of rat cardiac subcellular alterations induced by changing duration of noise stress. Anat. Rec., 248(4): 521-532.
35. Qian, L., X. Song, H. Ren, J. Gong and S. Cheng, 2004. Mitochondrial mechanism of heat stress-induced injury in rat cardiomyocyte. Cell Stress Chaperones Autumn, 9(3): 281-293.
36. Gehan, M.S. and M.T. Sadika, 2014. Histological and immunohistochemical study on the effect of aflatoxin B1 on the left ventricular muscle of adult male rabbit with reference to the protective role of melatonin. Egyptian Journal of Histology, 37: 655-666.
37. Savi, M., S. Rossi, L. Bocchi, L. Gennaccaro, F. Cacciani, A. Perotti, D. Amidani, R. Alinovi, M. Goldoni, I. Aliatis, P.P. Lottici, D. Bersani, M. Campanini, S. Pinelli, M. Petyx, C. Frati, A. Gervasi, K. Urbanek, F. Quaini, A. Buschini, D. Stilli, C. Rivetti, E. Macchi, A. Mutti, M. Miragoli and M. Zaniboni, 2014. Titanium dioxide nanoparticles promote arrhythmias via a direct interaction with rat cardiac tissue. Particle and Fibre Toxicology, 11: 63.
38. Ostrowski, A., D. Nordmeyer, A. Boreham and C. Holzhausen, 2015. Overview about the localization of nanoparticles in tissue and cellular context by different imaging techniques. Beilstein J. Nanotechnol., 6: 263-280.
39. Wim, H., C. De Jong Marina, A. Burger Marcel, Verheijen and E. Robert Geertsma, 2010. Detection of the Presence of Gold Nanoparticles in Organs by Transmission Electron Microscopy. Materials, 3: 4681-4694.